

High-speed directly modulated distributed feedback laser based on detuned loading and photon-photon resonance effect

Yun-Shan Zhang(张云山), Yi-Fan Xu(徐逸帆), Ji-Lin Zheng(郑吉林), Lian-Yan Li(李连艳), Tao Fang(方涛), and Xiang-Fei Chen(陈向飞)

Citation: Chin. Phys. B, 2023, 32 (**9**): 094204. DOI: 10.1088/1674-1056/acc8c1
Journal homepage: http://cpb.iphy.ac.cn; http://iopscience.iop.org/cpb

What follows is a list of articles you may be interested in

Single-frequency linearly polarized *Q*-switched fiber laser based on Nb_2GeTe_4 saturable absorber

Si-Yu Chen(陈思雨), Hai-Qin Deng(邓海芹), Wan-Ru Zhang(张万儒), Yong-Ping Dai(戴永平), Tao Wang(王涛), Qiang Yu(俞强), Can Li(李灿), Man Jiang(姜曼), Rong-Tao Su(粟荣涛), Jian Wu(吴坚), and Pu Zhou(周朴)
Chin. Phys. B, 2023, 32 (**7**): 074203. DOI: 10.1088/1674-1056/acad6d

A 54-fs diode-pumped Kerr-lens mode-locked Yb:$LuYSiO_5$laser

Yang Yu(于洋), Yuehang Chen(陈月航), Wenlong Tian(田文龙), Li Zheng(郑立), Geyang Wang(王阁阳), Chuan Bai(白川), Xuan Tian(田轩), Haijing Mai(麦海静), Yulong Su(苏玉龙), Jiangfeng Zhu(朱江峰), and Zhiyi Wei(魏志义)
Chin. Phys. B, 2023, 32 (**6**): 064204. DOI: 10.1088/1674-1056/acb9ed

Optically pumped wavelength-tunable lasing from a GaN beam cavity with an integrated Joule heater pivoted on Si

Feifei Qin(秦飞飞), Yang Sun(孙阳), Ying Yang(杨颖), Xin Li(李欣), Xu Wang(王旭), Junfeng Lu(卢俊峰), Yongjin Wang(王永进), and Gangyi Zhu(朱刚毅)
Chin. Phys. B, 2023, 32 (**5**): 054210. DOI: 10.1088/1674-1056/acc05e

Asymmetrical spiral spectra and orbital angular momentum density of non-uniformly polarized vortex beams in uniaxial crystals

Ling-Yun Shu(舒凌云), Ke Cheng(程科), Sai Liao(廖赛), Meng-Ting Liang(梁梦婷), and Ceng-Hao Yang(杨嶒浩)
Chin. Phys. B, 2023, 32 (**2**): 024211. DOI: 10.1088/1674-1056/ac7860

A cladding-pumping based power-scaled noise-like and dissipative soliton pulse fiber laser

Zhiguo Lv(吕志国), Hao Teng(滕浩), and Zhiyi Wei(魏志义)
Chin. Phys. B, 2023, 32 (**2**): 024207. DOI: 10.1088/1674-1056/ac8f3e

---

High-speed directly modulated distributed feedback laser based on detuned loading and photon–photon resonance effect

Yun-Shan Zhang(张云山)[1], Yi-Fan Xu(徐逸帆)[1], Ji-Lin Zheng(郑吉林)[2], Lian-Yan Li(李连艳)[1], Tao Fang(方涛)[3], and Xiang-Fei Chen(陈向飞)[3,†]

[1] *College of Electronic and Optical Engineering & College of Flexible Electronics (Future Technology), Nanjing University of Posts and Telecommunications, Nanjing* 210023, *China*

[2] *College of Communications Engineering, PLA Army Engineering University, Nanjing* 210007, *China*

[3] *College of Engineering and Applied Sciences, Nanjing University, Nanjing* 210023, *China*

(Received 30 December 2022; revised manuscript received 17 March 2023; accepted manuscript online 30 March 2023)

A monolithic integrated two-section distributed feedback (TS-DFB) semiconductor laser for high-speed direct modulation is proposed and analyzed theoretically. The grating structure of the TS-DFB laser is designed by the reconstruction-equivalent-chirp (REC) technique, which can reduce the manufacturing cost and difficulty, and achieve high wavelength controlling accuracy. The detuned loading effect and the photon–photon resonance (PPR) effect are utilized to enhance the modulation bandwidth of the TS-DFB laser, exceeding 37 GHz, while that of the conventional one-section DFB laser is only 16 GHz. When the bit rate of the non-return-to-zero (NRZ) signal reaches 55 Gb/s, a clear eye diagram with large opening can still be obtained. These results show that the proposed method can enhance the modulation bandwidth of DFB laser significantly.

Keywords: directly modulated laser (DML), detuned loading effect, photon–photon resonance (PPR) effect, reconstruction-equivalent-chirp (REC) technique

PACS: 42.55.–f, 42.55.Px **DOI:** 10.1088/1674-1056/acc8c1

1. Introduction

Because of the explosive development of data communication services such as cloud computing, the data traffic over networks and the demands for large network bandwidth have been increasing rapidly. As the light sources of optical communication systems, high-speed modulated lasers are crucial in solving these problems. Compared with externally modulated lasers like electro-absorption modulator integrated lasers,[1,2] directly modulated lasers (DMLs) have the advantages of cost-effectiveness, small size, low power consumption, and high efficiency. Therefore, it is attractive to improve the modulation bandwidth of DML.

In order to realize high-speed DML, it is essential to increase the relaxation oscillation frequency of the laser. For this purpose, AlGaInAs is usually used instead of InGaAsP in the active region of the DML to obtain high differential gain.[3] Besides, by using buried heterostructure[4,5] and shortening the cavity length of the lasers[6–9] to reduce the volume of the active region, the relaxation oscillation frequency can also be enhanced. However, the buried heterostructure brings about the problem of active region oxidation and increases the manufacturing cost. Moreover, in order to obtain an extremely short cavity length, it is usually necessary to combine various complex processes or structures. Through integrating a distributed feedback (DFB) laser with a passive waveguide[7,8] or passive distributed reflectors,[9] the length of the active region can be reduced beyond the limit of the cleaving process. While the necessary butt-joint regrowth process when fabricating these structures increases fabrication cost and difficulty.

In addition to reducing the active region of the laser, other modulation bandwidth enhancement methods can be used to design high-speed DML. One of them is the detuned loading effect,[10] which is common in conventional distributed Bragg reflector (DBR) lasers.[11,12] When lasing occurs on the long wavelength flank of the DBR mirror, the detuned loading effect can increase the resonance frequency of the laser.[13] The photon–photon resonance (PPR) effect is also widely utilized to improve the bandwidth of DML.[14–16] The interaction between the main mode and an adjacent cavity mode can produce a second resonance peak with a much higher frequency than relaxation oscillation. In a passive feedback laser (PFL),[14] the DFB laser is integrated with a passive feedback section. The PPR effect is generated by injecting current into the feedback section to optimize the phase. The above two effects can coexist in both DBR laser[17] and distributed reflector (DR) laser.[18,19] Therefore, the combination of the two effects can further increase the modulation bandwidth. Similarly, the integration of the active section and the passive section increases the difficulty and cost of chip manufacturing.

In this paper, we propose and demonstrate theoretically a two-section DFB (TS-DFB) laser with sampled Bragg gratings (SBGs). The TS-DFB laser consists of two sections: one plays

[†]Corresponding author. E-mail: chenxf@nju.edu.cn

© 2023 Chinese Physical Society and IOP Publishing Ltd

a role of a general DFB laser, and the other acts as a grating reflector. For simplicity, they are called section I and section II, respectively. Both sections share the same active layer, so the butt-joint regrowth is not required. In order to enhance the modulation bandwidth of the laser, the grating period of the two sections needs to be controlled accurately to achieve the detuned loading effect and PPR effect. The SBGs in the TS-DFB laser are used to realize the equivalent change of the period of the seed grating by using the reconstruction-equivalent-chirp (REC) technique.[20–22] Consequently, the cost of manufacturing can be greatly reduced. The simulation results show that the direct modulation bandwidth of TS-DFB laser can be improved by 21 GHz or more compared with the conventional one-section DFB (OS-DFB) laser.

2. Principle and model

2.1. Principle of REC technique

In order to improve the characteristics of the DFB lasers, various complicated grating structures (e.g. multiple phase shifts gratings, corrugation-pitch-modulated gratings, and asymmetric gratings) have been developed and used. Yet high-precision control mechanism is indispensable to the fabrication of these sophisticated gratings. Through changing the period or duty cycle of the SBGs, the REC technique can design equivalent subgratings with many complicated structures. Besides, the fabrication of SBGs only needs the conventional holographic exposure and photolithography technology with micrometer-level control accuracy. The principle of the REC technique will be briefly introduced below.[23,24]

Mathematically, the index modulation changes $\Delta n(z)$ of an SBG can be written as

$$\Delta n\left(z\right)=\frac{1}{2}s\left(z\right)\exp\left(\mathrm{j}\frac{2\pi z}{\Lambda}\right)+\mathrm{c.c.}, \tag{1}$$

where, $s(z)$ is a sampling function and Λ is the period of the seed grating. Based on the Fourier series expansion, $s(z)$ can be expressed as

$$s\left(z\right)=\sum_{m}F_{m}\exp\left(\mathrm{j}\frac{2m\pi z}{P}\right), \tag{2}$$

where F_m is the m-th order Fourier coefficient corresponding to the m-th order channel of the SBG, and P is the sampling period of the sampling function. So, equation (1) can be expressed as

$$\Delta n\left(z\right)=\sum_{m}\frac{1}{2}F_{m}\exp\left[\mathrm{j}\left(\frac{2\pi z}{\Lambda}+\frac{2m\pi z}{P}\right)\right]+\mathrm{c.c.} \tag{3}$$

It can be obtained from Eq. (3) that the SBG is actually a superposition of many subgratings with different grating periods, and every subgrating has a spectral response corresponding to one of the multiple channels. These periods can be expressed as

$$\Lambda_{m}=\frac{P\Lambda}{P+m\Lambda}. \tag{4}$$

From Eq. (4), the channel spacing is determined by the sampling period P. In actual design, the $+1$st or -1st subgrating is used as the working resonator. An appropriate sampling period P should be selected such that the $+1$st or -1st channel falls within the gain spectrum of the semiconductor material, while the others are located outside the gain region. As a result, the laser will lase at the wavelength within the $+1$st or -1st order channel of the SBG.

Now, $+1$st channel is taken as an example. Based on Eq. (4), the period of seed grating Λ and the sampling period P satisfy

$$\frac{2n_{\mathrm{eff}}}{\lambda}=\frac{P+\Lambda}{P\Lambda}, \tag{5}$$

where n_{eff} is the effective refractive index, and λ is the lasing wavelength.

2.2. Model of the simulation

The time-domain traveling-wave model consists of the time-dependent coupled-wave equations and the carrier rate equation to simulate the lasing characteristics of the proposed TS-DFB laser.[25,26] The electrical field in the waveguide can be described as

$$\boldsymbol{E}\left(x,y,z,t\right)=\phi\left(x,y\right)\left[F\left(z,t\right)\mathrm{e}^{-\mathrm{i}\beta_{0}z}+R\left(z,t\right)\mathrm{e}^{\mathrm{i}\beta_{0}z}\right]\mathrm{e}^{\mathrm{i}\omega_{0}t}, \tag{6}$$

where $\phi(x,y)$ is the model function in the waveguide, $F(z,t)$ and $R(z,t)$ represent the forward wave and backward wave propagating in the waveguide respectively, β_0 is the propagation constant at Bragg frequency, and ω_0 is the reference frequency corresponding to the Bragg wavelength λ_0. The fields $F(z,t)$ and $R(z,t)$ satisfy the time-dependent coupled-wave equations:

$$\begin{aligned}&\frac{1}{v_{\mathrm{g}}}\frac{\partial F\left(z,t\right)}{\partial t}+\frac{\partial F\left(z,t\right)}{\partial z}\\&=\left(G-\mathrm{i}\delta\right)F\left(z,t\right)+\mathrm{i}\kappa R\left(z,t\right)+s_{\mathrm{F}}\left(z,t\right),\end{aligned} \tag{7a}$$

$$\begin{aligned}&\frac{1}{v_{\mathrm{g}}}\frac{\partial R\left(z,t\right)}{\partial t}-\frac{\partial R\left(z,t\right)}{\partial z}\\&=\left(G-\mathrm{i}\delta\right)R\left(z,t\right)+\mathrm{i}\kappa^{*}F\left(z,t\right)+s_{\mathrm{R}}\left(z,t\right).\end{aligned} \tag{7b}$$

Here, v_{g} is the group velocity. G and δ are the field gain and the detuning factor respectively, and κ is the coupling coefficient between forward and backward waves. In this work, we consider only index coupling. The $s_{\mathrm{F}}(z,t)$ and $s_{\mathrm{R}}(z,t)$ are the spontaneous emission noise coupled into the forward and backward fields. The noise terms each have a Gaussian distribution and the phase of the noise is assumed to change randomly.

The carrier density N is described by the time-dependent carrier rate equation as

$$\frac{\mathrm{d}N}{\mathrm{d}t} = \frac{J}{ed} - AN(z,t) - BN(z,t)^2 - CN(z,t)^3 - \frac{v_g g \ln(N(z,t)/N_0) S}{(1+\varepsilon S)}, \tag{8}$$

where J is the current injection density, e is the electron charge, d is the thickness of the active layer, A is the linear recombination coefficient, B is the bimolecular recombination coefficient, C is the Auger recombination coefficient, g is the gain coefficient, N_0 is the transparency carrier density, ε is the gain compression factor, and S is the photon density which is related to the magnitude of the propagating wave amplitudes as

$$S(z,t) = |F(z,t)|^2 + |R(z,t)|^2. \tag{9}$$

The field gain G in Eqs. (7a) and (7b) is expressed as

$$G(z,t) = \frac{\Gamma g \ln(N(z,t)/N_0)}{2(1+\varepsilon S)} - \frac{\alpha}{2}, \tag{10}$$

where Γ is the confinement factor of the active layer, and α is the waveguide loss caused by free electron scattering and absorption.

The detuning factor δ in Eqs. (7a) and (7b) represents the deviation from the Bragg condition due to the change of the refractive index in the waveguide and can be defined as

$$\delta = \frac{\omega_0}{c}(n_{\mathrm{eff0}} + \Delta n) - \frac{\pi}{\Lambda}, \tag{11}$$

where n_{eff0} is the effective refractive index at transparency, Δn is the change of the refractive index and can be written as

$$\Delta n = -\frac{\lambda_0}{4\pi}\Gamma \alpha_{\mathrm{H}} g \ln(N(z,t)/N_0), \tag{12}$$

where α_{H} is the linewidth enhancement factor.

If $z = 0$ at the facet on the left-hand side, the boundary condition for the forward and backward propagating wave at the facet satisfies

$$F(0,t) = r_{\mathrm{l}} \exp(\mathrm{j}\varphi_{\mathrm{l}}) R(0,t), \tag{13a}$$

$$R(L,t) = r_{\mathrm{r}} \exp(\mathrm{j}\varphi_{\mathrm{r}}) F(L,t), \tag{13b}$$

where r_{l} and r_{r} are the amplitude of the reflectivity at the facets on the left- and the right-hand sides, respectively, φ_{l} and φ_{r} are the phase at the facets on the left- and the right-hand sides, and L is the laser cavity length.

In this work, we focus on the DFB lasers fabricated by REC technology. Hence, the grating in the simulation is a sampled grating. In the part without change of the refractive index, we set the coupling coefficient $\kappa = 0$. According to Eq. (5), it satisfies in our simulation that

$$\frac{2n_{\mathrm{eff0}}}{\lambda_0} = \frac{P_{\mathrm{l}} + \Lambda}{P_{\mathrm{l}}\Lambda}, \tag{14}$$

where P_{l} is the sampling period of section I and can be calculated from the Bragg wavelength λ_0 and the period of seed grating Λ through Eq. (14).

For section II, only the sampling period instead of the period of the seed grating Λneeds to be changed, thereby reducing the difficulty of fabrication.

3. Design principle and simulation results

3.1. Design of TS-DFB laser

The proposed structure of the TS-DFB laser is shown in Fig. 1(a). It consists of two sections separated by electrical isolation. Therefore, two regions can be independently injected by different currents I_1 and I_2. Section I works as a general DFB laser, and the other serves as a detuned grating reflector. Moreover, the two sections share the same active layer, so the butt-joint regrowth process is avoidable. The facet of section I is high-reflection (HR) coated and the facet of section II is anti-reflection (AR) coated. The light is output after passing through the grating reflector. The reflectivity of the HR coating is set to 0.92. Figure 1(b) shows the grating structure fabricated by the REC technique in the two sections. The SBGs in the two sections have the identical coupling coefficient κ and seed grating period Λ. The only difference is that the gratings of the two sections have distinct sampling periods, denoted as P_1 and P_2 respectively. In the simulation, the equivalent normalized coupling coefficient of the SBGs is set to 1, where the duty cycle of the sampled gratings is considered. The duty cycle of the SBGs is 0.5. Other parameters used in the simulation are given in Table 1.

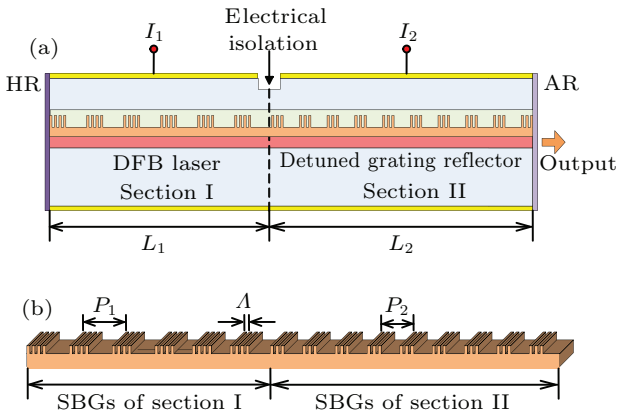


Fig. 1. Schematic diagram of (a) proposed TS-DFB laser and (b) grating structure of the TS-DFB laser.

In order to make better use of the detuned loading and the PPR effects to enhance the modulation bandwidth of the TS-DFB laser, the SBGs in the two sections need different sampling periods, that is, detuning between the grating Bragg wavelengths in the two sections is realized. Figure 2 shows the reflection spectrum of the grating reflector and the round trip phase of the laser, which are calculated by the transfer matrix

method[27,28] after the effective refractive index and gain distribution in the laser cavity have been obtained from the time-domain traveling-wave model. The detuning of the gratings can make the main mode fall on the long wavelength flank of the reflection spectrum. Under modulation, the frequency up-chirp of the TS-DFB laser shifts the main mode to the Bragg peak of section II. The longitudinal confinement factor is increased. As a result, the detuned loading effect can increase the resonance frequency.[11] Moreover, the side mode which is close to the main mode can resonantly amplify the modulation sidebands. Thus, PPR effect can further improve the 3-dB bandwidth.

Table 1. Parameters used in simulations.

Parameter	Symbol	Value
Length of section I	L_1	400 μm
Length of section II	L_2	500 μm
Thickness of the active layer	d	48 nm
Width of the active layer	w	2 μm
Period of the seed grating	Λ	252.03 nm
Sampling period of section I	P_1	5 μm
Sampling period of section II	P_2	4.968 μm
Duty cycle of the sampled grating	R_d	0.5
Equivalent normalized coupling coefficient	κL_1	1
Effective refractive index at transparency	n_{eff0}	3.23
Group refractive index	n_g	3.6
Linear recombination coefficient	A	1×10^{9} s^{-1}
Bimolecular recombination coefficient	B	1×10^{-10} cm^3·s^{-1}
Auger recombination coefficient	C	7.5×10^{-29} cm^6·s^{-1}
Spontaneous coupling factor	β	2.5×10^{-5}
Gain coefficient	g	1100 cm^{-1}
Waveguide loss	α	10 cm^{-1}
Confinement factor	Γ	0.1
Gain compression factor	ε	4×10^{-17} cm^3
Linewidth enhancement factor	α_H	2
Transparency carrier density	N	1×10^{18} cm^{-3}
Reflectivity of the AR coating	R_{AR}	0
Reflectivity of the HR coating	R_{HR}	0.92

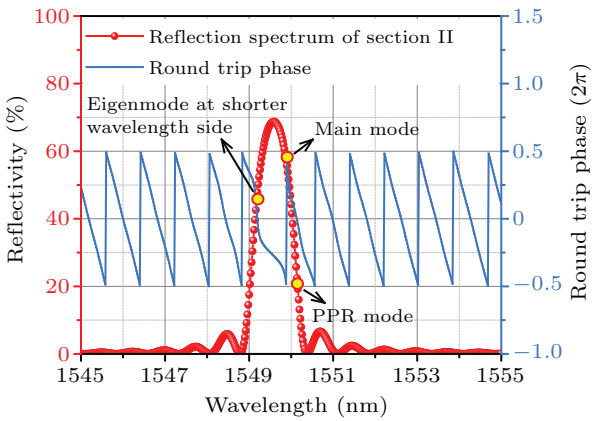


Fig. 2. Reflection spectrum of detuned grating reflector and round trip phase of the laser, with the positions of the modes in profiles represented by circles.

3.2. Static characteristics of the TS-DFB laser

Figure 3(a) shows the longitudinal photon density distribution of the TS-DFB laser when the injection current I_1 is 100 mA. Since the light of the TS-DFB laser is output from the grating reflector side, the photon density will be reduced due to the absorption loss and reflection, implying a lower output power. The bias current I_2 can be added to the reflector section to compensate for the loss and increase the output. Thus, the photon density at the output facet of the TS-DFB laser will become higher. The light–current characteristics of the TS-DFB laser are shown in Fig. 3(b). It can be seen that the bias current I_2 has a great influence on the light–current characteristics of the TS-DFB laser. When I_2 increases, the threshold current decreases and the slope efficiency increases. The threshold currents of the TS-DFB laser are about 22 mA for $I_2 = 0$ mA and 9 mA for $I_2 = 10$ mA, and correspondingly the slope efficiencies are about 0.248 mW/mA and 0.277 mW/mA.

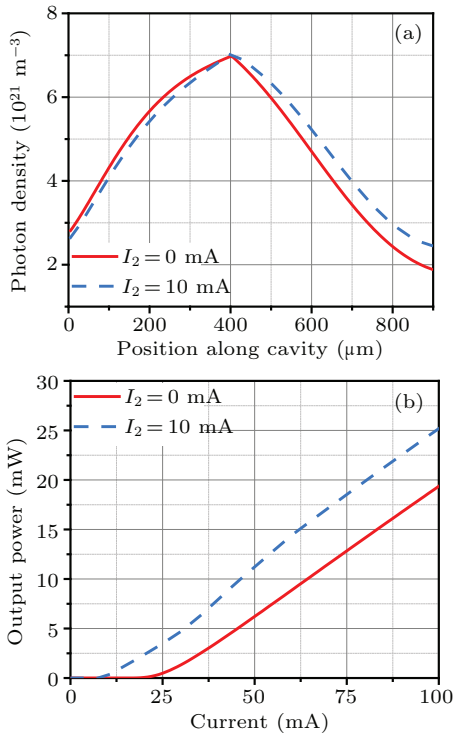


Fig. 3. (a) Calculated photon density distribution of TS-DFB laser with injection current of 100 mA and (b) light–current characteristics of TS-DFB laser for $I_2 = 0$ mA and 10 mA.

The spectrum of the TS-DFB laser is shown in Fig. 4, which is calculated based on the model proposed in Ref. [29]. The side mode suppression ratio (SMSR) is 42 dB. Moreover, it can be seen that there is a side mode at about 0.2 nm off the main mode, which is named PPR mode. The PPR mode can improve the modulation bandwidth effectively, which is consistent with the laser design in Fig. 2.

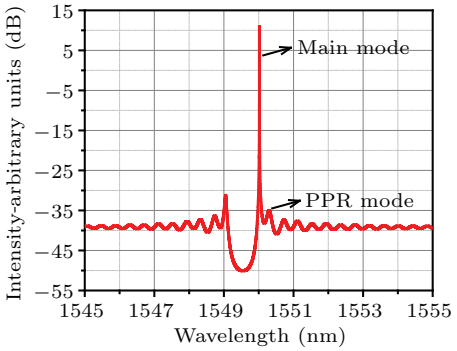


Fig. 4. Lasing spectrum of TS-DFB laser, with injection current being 100 mA.

3.3. Dynamic characteristics of TS-DFB laser

To calculate the small-signal modulation response of the TS-DFB laser, a small sinusoidal current is added to the bias current of section I. Figure 5 shows the response curves of the TS-DFB laser with different detunings of the grating Bragg wavelengths in the two sections. It is obvious that the detuning between the SBGs in the two sections has a significant influence on the modulation bandwidth of the TS-DFB laser. The larger detuning can make the main mode fall on the steeper Bragg wavelength flank of section II, which can enhance the detuned loading effect. Therefore, the resonance frequency is improved. Moreover, it can generate and strengthen the PPR mode, so that the PPR effect can better generate a resonance frequency at high frequency.

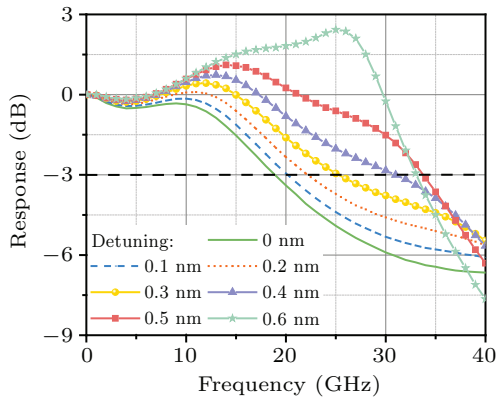


Fig. 5. Response curves of TS-DFB laser with different detunings between SBGs in the two sections, with I_1 being 100 mA.

The small-signal response curves of the TS-DFB laser with different values of injection current I_2 are shown in Fig. 6(a). For comparison, the response of the conventional OS-DFB laser with a cavity length of 400 μm is also given. The 3-dB modulation bandwidth of the OS-DFB laser is only about 16 GHz. However, for the TS-DFB laser, it can be seen that the detuned loading effect enhances the resonance frequency, and the PPR effect forms a second resonance peak on the response curve. The modulation bandwidth increases from 34 GHz to 37 GHz when I_2 is tuned from 0 mA to 15 mA. The increase of the reflection of the grating reflector enhances the resonance strength of the PPR peak. When I_2 is 20 mA, the mode hops from the long wavelength flank of the Bragg peak to the short wavelength flank as shown in Fig. 6(b). This is because with the increase of I_2, the effective index of section II decreases, and the reflection spectrum moves towards the short wavelength. In this situation, the detuned loading effect is absent. The mode spacing is too large, so the PPR effect does not work. Therefore, the modulation bandwidth is attenuated to 15.5 GHz. Hence, a current large than 20 mA only makes the effective refractive index smaller and cannot improve the direct modulation bandwidth.

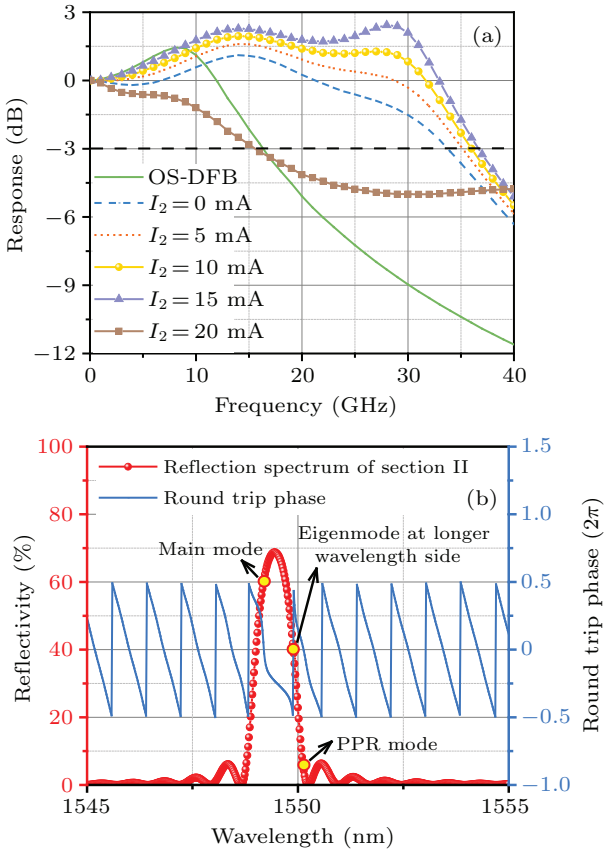


Fig. 6. (a) Response curves of TS-DFB laser, with I_1 being 100 mA and injection current I_2 having different values, and (b) reflection spectrum of grating reflector and round trip phase of the laser, with I_2 being 20 mA.

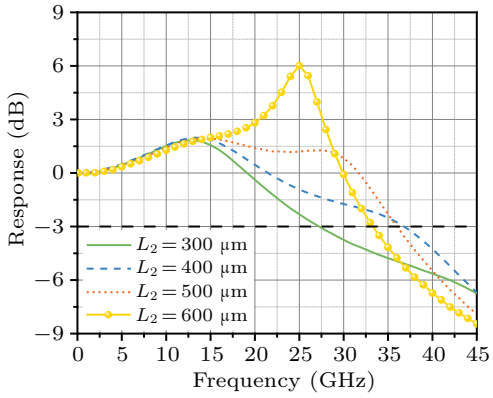


Fig. 7. Response curves of TS-DFB laser with different lengths of section II, with I_1 being 100 mA and I_2 being 10 mA.

The influence of the grating reflector length on the modulation response is illustrated in Fig. 7.

The separation between the main mode and the PPR mode is determined by the cavity length of grating reflector. The longer the grating reflector, the closer the PPR mode is to the main mode, and the overlap between the two resonance peaks becomes more and more. As shown in Fig. 7, when the cavity length of section II is 600 μm, the PPR mode is very close to the main mode, and the second resonance is very strong. When the length of section II is 400 μm, the spacing of the PPR mode from the main mode becomes larger, so the second resonance peak is at a higher frequency. However, the resonance strength

is weaker, due to the weaker feedback of the shorter grating reflector. When the length is further reduced, the PPR mode is too far away and too weak to increase the modulation bandwidth. Therefore, the length of the grating reflector should be appropriately designed to maximize the enhancement of the modulation bandwidth brought by the PPR effect.

In the above calculations, the random phase of the grating at the HR facet was set to 0. However, in practice, the phase randomness of the grating is uncontrollable. Therefore, facet phase φ is changed to study its effect on the high-speed modulation characteristics. Figure 8(a) shows the response curves of the TS-DFB laser when φ is varied from 0 to 0.8π. It can be seen that under certain phase conditions, mode hopping occurs and the modulation bandwidth is attenuated. When φ is 0.6π, the 3-dB bandwidth is only 21 GHz. In order to study the effect of the random phase on mode hopping, the normalized threshold gain margin between the eigenmode at the shorter wavelength side and the lasing mode is calculated, and the results are shown in Fig. 8(b). It can be seen that when the random phase is 0, the normalized threshold gain margin is less than 0.25. Therefore, when the current of the reflection section is too large, mode hopping occurs as shown in Fig. 6. The normalized threshold gain margin is 0 when the random phase is changed from 0.7π to 0.9π, which means that the lasing occurs at the eigenmode on the shorter wavelength side. Thus, the small-signal modulation response deteriorates.

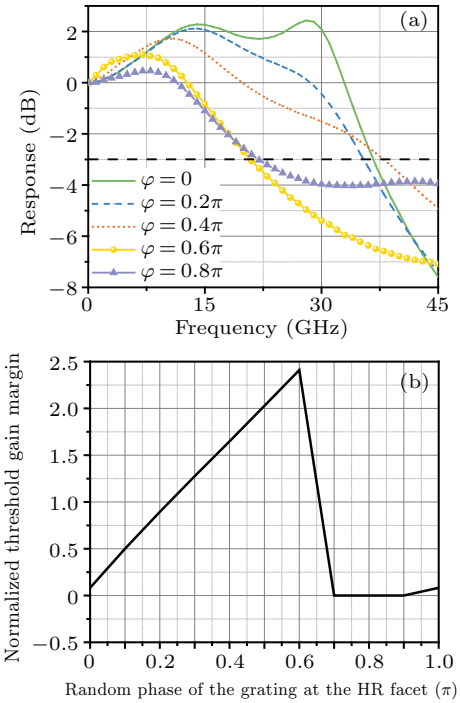


Fig. 8. (a) Response curves of TS-DFB laser with different values of facet phase φ with I_1 being 100 mA and I_2 being 15 mA. (b) Normalized threshold gain margin between the main mode and the eigenmode on the shorter wavelength side *versus* facet phase φ.

Figure 9(a) shows the lasing spectrum when φ is 0.6π. It can be seen that the main mode lases within the stopband due to the random phase of the grating. As a result, the spacing between the main mode and the PPR mode becomes larger. As can be seen from Fig. 9(b), the PPR frequency, in this case, is about 65 GHz, which is about 55 GHz larger than the first resonance peak. Because the two resonance peaks are too far apart, the response curve is attenuated below 3 dB before reaching the second resonance peak. Therefore, the PPR effect cannot improve the modulation bandwidth effectively. By increasing the current I_2, the loss of the grating reflector section is compensated for and the reflectivity is increased. Then the resonance strength of the PPR peak is enhanced, which counteracts the roll-off of the response. Consequently, the modulation bandwidth can reach around 73 GHz. Obviously, there are two PPR peaks in the response curves. The reason is that the multi-mode rate equation is used in the simulation, another resonance peak is caused by another side mode.

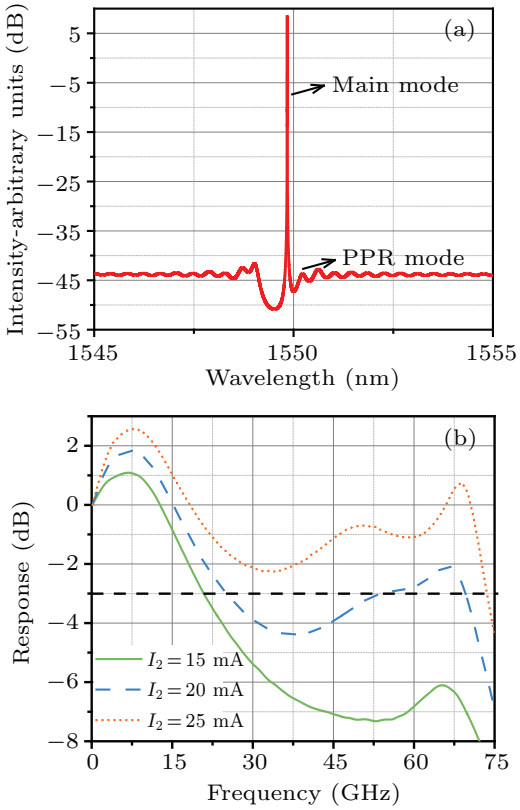


Fig. 9. (a) Lasing spectrum of TS-DFB laser, with φ being 0.6π. (b) Response curves of TS-DFB laser with I_2 having different values, I_1 being 100 mA, and φ being 0.6π.

In order to better demonstrate the high-speed characteristics of the TS-DFB laser, the eye diagrams under direct modulation are calculated and compared. Figure 10 shows the eye diagrams of the TS-DFB laser and the OS-DFB laser under 25-Gb/s, 40-Gb/s, and 55-Gb/s direct modulations. The lasers are biased at 100 mA and the modulation amplitude is 20 mA. The optimal bandwidth condition of the TS-DFB laser is selected,

and the random phase of the grating is 0. It can be seen that the eye diagrams of the TS-DFB lasers have larger opening extent than those of the OS-DFB laser. Under 25-Gb/s direct modulation, the clear eye-openings of two kinds of DFB lasers can be obtained owing to the enough modulation bandwidths. Obviously, the OS-DFB laser cannot meet the higher modulation rates. In contrast, the TS-DFB laser can achieve clear eye-openings and large mask margins under all three modulation rates. These results are consistent with the calculations of their modulation bandwidth in Fig. 6.

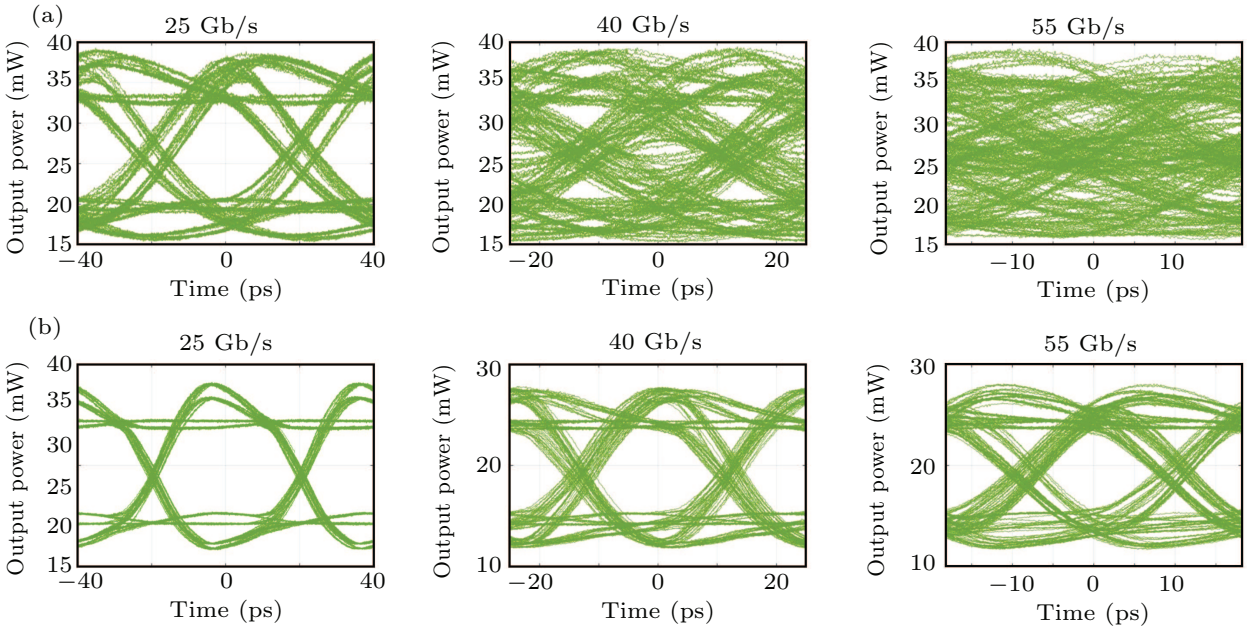


Fig. 10. Eye diagrams under direct modulation at 25 Gb/s, 40 Gb/s, and 55 Gb/s by (a) conventional OS-DFB laser and (b) TS-DFB laser.

4. Conclusions

A directly modulated two-section DFB laser with sampled gratings is proposed and investigated theoretically. Since the two sections share the same active layer and the gratings are fabricated by the REC technique, the difficulty in manufacturing the lasers is greatly reduced. High-speed DML is realized by exploiting the detuned loading, and PPR effects. Compared with the OS-DFB laser, the TS-DFB laser has large direct modulation bandwidth. Therefore, the proposed laser can be used as a light source for high-speed optical communication systems.

Acknowledgements

Project supported by the National Key Research and Development Program of China (Grant No. 2020YFB2205804), the National Natural Science Foundation of China (Grant Nos. 61974165 and Grant 61975075), and the National Natural Science Foundation of China for the Youth, China (Grant No. 62004105).

References

[1] Zhao Q, Pan J Q, Zhou F, Wang B J, Wang L F and Wang W 2005 *Chin. Phys. Lett.* **22** 2016

[2] Zhou D B, Wang H T, Zhang R K, Wang B J, Bian J, An X, Lu D, Zhao L J, Zhu H L, Ji C and Wang W 2015 *Chin. Phys. Lett.* **32** 054205

[3] Ishikawa T, Higashi T, Uchida T, Fujii T, Yamamoto T, Shoji H and Kobayashi M 1998 *International Conference on Indium Phosphide and Related Materials*, May 11–15, 1998, Tsukuba, Japan, p. 729

[4] Nakahara K, Wakayama Y, Kitatani T, Taniguchi T, Fukamachi T, Sakuma Y and Tanaka S 2015 *IEEE Photon. Technol. Lett.* **27** 534

[5] Otsubo K, Matsuda M, Takada K, Okumura S, Ekawa M, Tanaka H, Ide S, Mori K and Yamamoto T 2009 *IEEE J. Sel. Top. Quantum Electron.* **15** 687

[6] Kobayashi W, Tadokoro T, Ito T, Fujisawa T, Yamanaka T, Shibata Y and Kohtoku M 2012 *International Semiconductor Laser Conference*, October 7–10, 2012, San Diego, CA, USA, p. 50

[7] Sakaino G, Takiguchi T, Sakuma H, Watatani C, Nagira T, Suzuki D, Aoyagi T and Ishikawa T 2010 *22nd IEEE International Semiconductor Laser Conference*, September 26–30, 2010, Kyoto, Japan, p. 197

[8] Tadokoro T, Kobayashi W, Fujisawa T, Yamanaka T and Kano F 2012 *J. Lightwave Technol.* **30** 2520

[9] Uetake A, Otsubo K, Matsuda M, Okumura S, Ekawa M and Yamamoto T 2009 *IEEE LEOS Annual Meeting Conference Proceedings*, October 4–8, 2009, Belek-Antalya, Turkey, p. 839

[10] Vahala K and Yariv A 1984 *Appl. Phys. Lett.* **45** 501

[11] Chacinski M, Schatz R and Kjebon O 2004 *Proceedings of* 2004 *International Students and Young Scientists workshop Photonics and Microsystems*, September 8–10, 2004, Acapulco, Mexico, p. 1

[12] Kjebon O, Schatz R, Lourdudoss S, Nilsson S, Stålnacke B and Bäckbom L 1997 *Electron. Lett.* **33** 488

[13] Matsui Y, Schatz R, Che D, Khan F, Kwakernaak M and Sudo T 2021 *Nat. Photon.* **15** 59

[14] Kreissl J, Vercesi V, Troppenz U, Gaertner T, Wenisch W and Schell M 2012 *IEEE Photon. Technol. Lett.* **24** 362

[15] Feiste U 1998 *IEEE J. Quantum Electron.* **34** 2371

[16] Morthier G, Schatz R and Kjebon O 2000 *IEEE J. Quantum Electron.* **36** 1468

[17] Kjebon O, Schatz R, Lourdudoss S, Nilsson S, Stalnacke B and Backbom L 1997 *International Conference on Indium Phosphide and Related Materials*, May 11–15, 1997, Cape Cod, MA, USA, p. 665

[18] Matsui Y, Pham T, Ling W A, Schatz R, Carey G, Daghighian H, Sudo T and Roxlo C 2016 *Optical Fiber Communications Conference and Exhibition*, March 20–24, 2016, Anaheim, CA, USA, p. 1

[19] Matsui Y, Schatz R, Pham T, Ling W A, Carey G, Daghighian H M, Adams D, Sudo T and Roxlo C 2017 *J. Lightwave Technol.* **35** 397

[20] Zhang Y S, Zheng J L, Shi Y C, Qian Y J, Zheng J S, Zhang F Z, Wang P, Qiu B C, Lu J, Wang W X and Chen X F 2015 *IEEE J. Sel. Top. Quantum Electron.* **21** 232

[21] Yuan B C, Shi J Q, Qi W X, Li L Y, Zheng J L, Xiao R L, Shi Y C, Chen X F, Xu N and Zhang Y S 2020 *IEEE Photon. J.* **12** 1

[22] Guan S J, Zhang Y S, Yuan B C, Li L Y, Wang C S, Zheng J L, Fang T, Shi Y C, and Xiao R L and Chen X F 2021 *J. Lightwave Technol.* **39** 4725

[23] Dai Y T, Chen X F, Xia L, Zhang Y J and Xie S Z 2004 *Opt. Lett.* **29** 1333

[24] Dai Y T and Yao J P 2008 *IEEE J. Quantum Electron.* **44** 938

[25] Zhang L M, Yu S F, Nowell M C, Marcenac D D, Carroll J E and Plumb R G S 1994 *IEEE J. Quantum Electron.* **30** 1389

[26] Kim B S, Kim J K, Chung Y and Kim S H 1998 *IEEE Photon. Technol. Lett.* **10** 39

[27] Wang H, Zhu H L, Jia L H, Chen X F, Li J S and Wang W 2008 *Chin. Phys. Lett.* **25** 4162

[28] Wang H, Zhu H L, Jia L H, Chen X F, Kong D H, Wang L S, Zhang W, Zhao L J and Wang W 2009 *Chin. Phys. B* **18** 2868

[29] Morrison G B and Cassidy D T 2000 *IEEE J. Quantum Electron.* **36** 633